International Journal of Naval Architecture and Ocean Engineering
Volume 9, Issue 2, March 2017, Pages 149-159

Numerical study of ship motions and added resistance in regular incident waves of KVLCC2 model

Yavuz Hakan Ozdemir [a, 1], Baris Barlas [b]

https://doi.org/10.1016/j.ijnaoe.2016.09.001

Abstract

In this study, the numerical investigation of ship motions and added resistance at constant forward velocity of KVLCC2 model is presented. Finite volume CFD code is used to calculate three dimensional, incompressible, unsteady RANS equations. Numerical computations show that reliable numerical results can be obtained in head waves. In the numerical analyses, body attached mesh method is used to simulate the ship motions. Free surface is simulated by using VOF method. The relationship between the turbulence viscosity and the velocities are obtained through the standard $k-\varepsilon$ turbulence model. The numerical results are examined in terms of ship resistance, ship motions and added resistance. The validation studies are carried out by comparing the present results obtained for the KVLCC2 hull from the literature. It is shown that, ship resistance, pitch and heave motions in regular head waves can be estimated accurately, although, added resistance can be predicted with some error.

Keywords

Ship motions; RANSE; Turbulent free surface flows; Added wave resistance

1. Introduction

The use of numerical models for predicting the ship performance in preliminary design step is getting in common. The model experiments are still very valuable; hence, time and cost encourage the use of Computational Fluid Dynamics (CFD). In the past, CFD approaches were based on potential flow theory because the Navier–Stokes equation was difficult to solve. There are some approaches in solving Navier–Stokes equations, but recent developments in computing technology enable researchers to solve the problems in shipbuilding industry by means of Reynolds-Averaged Navier–Stokes (RANS) equations.

The prediction of added resistance of a ship in waves is important for the ship's performance and seakeeping. Some methods can be found in the literature, but the most reliable ones are based on the linear strip theory of Salvesen et al. (1970). Many studies practiced potential flow methods used in hydrodynamics (Salvesen, 1978, Faltinsen et al., 1980). Recently, RANS methods gain advantage. Several researchers have studied the motions and added resistance of a ship. Some of these studies were based on potential theory, others were based on RANS. Furthermore, most of the work done was restricted to regular head waves. Fang (1998) developed a robust method to calculate the added resistance of SWATH ships advancing in regular waves. Modeling of free surface flows around different test cases have been reported by Sato et al. (1999), by using RANS equation. The well-known strip theory was still used in his method. Orihara and Miyata (2003) developed a CFD method using RANS equations to estimate the added resistance of ships in waves. Some methods that can be used to predict the added resistance of a monohull ship were investigated and validated by means of the experimental study of Arribas (2007). Wilson et al. (2006), simulated roll decay motion by using unsteady RANS equation. A flow-simulation method was developed to predict the performance of a high-speed vessel in unsteady motion on a free surface by Panahani et al. (2009). The ship motion conditions of the high-speed vessel are virtually realized by combining the simulations of water-flow and the motion of the vessel. Deng et al. (2010) use a RANS solver using Finite Volume (FV) discretization and free surface capturing approach. In this study, it was shown that special attention required for time discretization. Matulja et al. (2011) estimated the added resistance of four different merchant ships by using three different methods and compare them with the experiments. The added resistance of KVLCC2 in small amplitude short and regular waves ($1.090 \le L/\lambda \le 5.526$) were investigated using strip theory and experimentally by Guo and Steen (2011). Liu et al. (2011) estimated the added resistance of ships using a 3D panel, and time-domain Rankine source-Green function methods, and validated the applicability of the implemented methods by using wide range of hull forms. Guo et al. (2012) presented to the prediction of added resistance and ship motion of KVLCC2 model in head waves by using RANS equation. The motions and added resistance of KVLCC2 at two different Froude numbers with free and fixed surge in short ($2.091 \le L/\lambda \le 5.525$) and long ($1.67 \le L/\lambda \le 0.5$) head waves were predicted using URANS by Sadat-Hosseini et al. (2013) and verifications showed that the results were fairly insensitive to the grid size and the time step. Zhirong and Decheng (2013) investigated the added resistance, heave and pitch motions in head waves using RANS. Masashi (2013) investigated the effects of nonlinear ship-generated unsteady waves, ship motions and added resistance by using blunt and slender Wigley forms. It was found that near the peak value of added resistance the degree of nonlinearity in the unsteady wave became noticeable. Seo et al. (2013) studied on the comparison of the computation of added resistance and validation with experimental data on Wigley and Series 60 hulls, and S175 container ship. They used three different methods; the Rankine panel, strip theory, and Cartesian grid.

In the present study, two different physical problems of the KVLCC2 container ship is examined: total ship resistance modeled in calm water and the free heave and pitch motion response due to the incident waves. The KVLCC2 was designed at the Korea Research Institute for Ships and Ocean Engineering (now MOERI) around 1997 to be used as a test case for CFD predictions. KVLCC2 was selected as a test case in the Gothenburg 2010 CFD workshop (G2010, 2010). Both free heave and pitch motion in head waves are performed. The ship resistances in waves are also analyzed. The added resistance is calculated by subtracting the steady surge force from the mean surge force calculated from the equations of motion. The present work is performed to show the capability of general purpose CFD code of Star CCM + for design, analysis and reliability, and to carry out validation analysis on a personal computer. The finite volume solution method for the RANS equation is applied to the unsteady turbulent flow simulation. The turbulence model used is the well-known standard $k-\varepsilon$ two-equation turbulence model. The next section of this paper provides brief explanations about the governing equations, boundary conditions, computations, validation, and conclusions.

2. Geometry and conditions

As the KVLCC2 hull form is used for seakeeping and total resistance simulations, the geometry of the KVLCC2 ship model is given in Fig. 1. G is the center of gravity, which is the origin of a ship-fixed reference frame, it is set in the plane of the undisturbed free surface; the z axis is the vertical direction, positive upward, the x axis is in the aft direction, and y the lateral direction. In order to evaluate the numerical and experimental results, a right-handed coordinate system is used (Panahani et al., 2009). The model hull does not have a rudder and a propeller. The KVLCC2 model has a scale of 1/58 that is implemented for the numerical calculations. Table 1 gives the model ship and main ship particulars.

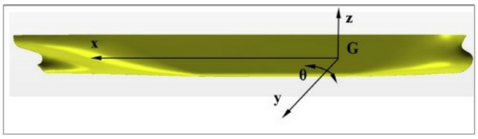

Fig. 1. KVLCC2 geometry for pitch and heave in head waves at constant forward speed.

Table 1. Geometrical properties of KVLCC2.

	Symbol	Ship	Model
Scale	**λ**	**1**	**58**
Length between perpendiculars	L_{PP} (m)	320.0	5.5172
Maximum beam of waterline	B (m)	58.0	1.0000
Draft	T (m)	20.8	0.3586
Block coefficient	C_B	0.8098	0.8098
Displacement	∇ (m^3)	312,622	1.6023
Moment of inertia	K_{xx}/B	0.40	0.40
Moment of inertia	K_{yy}/L_{PP}, K_{zz}/L_{PP}	0.25/0.25	0.25/0.25
Froude number	Fr	0.142	0.142
Speed	U (m/s)	7.973	1.044

Guo et al. (2012) have investigated sinkage and trim of KVLCC2 container ship. They showed that sinkage and trim values of KVLCC2 are very small. For this reason in this study model fixed from its floating position and it is not free to sinkage and trim, their effects on ship resistance are neglected. During the ship motion analysis, the pitching and heaving motions are free, and other motions are not permitted. Both ship motion and ship resistance simulation, the effect of the wind is not taken into account. Three different seakeeping simulation conditions are given in Table 2. U is the ship speed, f is the wave frequency, f_e is the encounter frequency, λ is the wave length and ζ is the wave amplitude.

Table 2. Coupled pitch and heave simulation conditions.

Condition no.	**C1**	**C2**	**C3**
Froude number (Fr)	0.142	0.142	0.142
Wave length λ/L_{PP}	0.9171	1.1662	1.600
Wave amplitude ζ (mm)	75	75	75
Wave frequency f (Hz)	0.555	0.492	0.420
Encounter frequency f_e (Hz)	0.761	0.654	0.538

3. Mathematical formulation

3.1. Governing equations

The equation for the translation of the center of mass of the ship body is given as;

$$m\frac{dv}{dt} = f \tag{1}$$

where m represents the mass of the body, f is the resultant force acting on the body and v is the velocity of the center of mass. An angular momentum equation of the body is formulated in the body local coordinate system with the origin in the center of the body;

$$M\frac{d\omega}{dt} + \omega \times M\omega = n \tag{2}$$

where M is the tensor of moments of inertia, ω is the angular velocity of rigid body, and n is the resultant moment acting on the body. The resulting force and moment acting on the ship are obtained from fluid pressure and shear force acting on the each boundary face of the body. The translations of the ship are estimated according the computed velocity and pressure fields in the flow domain. A more detailed discussion of this point is provided in (Panahani et al., 2009).

The governing equations are the RANS equations and the continuity equation for mean velocity of the unsteady, three-dimensional incompressible flow. The continuity equation and momentum equations in Cartesian coordinates can be given as:

$$\frac{\partial U_i}{\partial x_j} = 0 \tag{3}$$

for the continuity,

$$\frac{\partial U_i}{\partial t} + \frac{\partial (U_i U_j)}{\partial x_j} = -\frac{1}{\rho}\frac{\partial P}{\partial x_i} + \frac{\partial}{\partial x_j}\left[\nu\left(\frac{\partial U_i}{\partial x_j} + \frac{\partial U_j}{\partial x_i}\right)\right] - \frac{\partial\left(\overline{u_i' u_j'}\right)}{\partial x_j} \tag{4}$$

for the momentum equations, where U_i and u_i' express the mean and fluctuation velocity component in the direction of the Cartesian coordinate x_i, p the mean pressure, ρ the density and ν the kinematic viscosity. The Reynolds stress tensor is then calculated by using the well-known Boussinesq model:

$$\overline{u_i' u_j'} = -\nu_t\left(\frac{\partial U_i}{\partial x_j} + \frac{\partial U_j}{\partial x_i}\right) + \frac{2}{3}\delta_{ij}k \tag{5}$$

The eddy viscosity ν_t is expressed as $\nu_t = C_\mu k^2/\varepsilon$, where C_μ is an empirical constant $(C_\mu = 0.09)$, k the turbulent kinetic energy and ε the dissipation rate of k. The turbulence quantities k and ε are then computed from a $k - \varepsilon$ model using two transport equations. The well-known standard $k - \varepsilon$ two-equation turbulence model has been used to simulate the turbulent flows. The turbulent kinetic energy, k, and the rate of dissipation of the turbulent energy, ε are (Chau et al., 2005):

$$\frac{\partial k}{\partial t} + \frac{\partial (kU_j)}{\partial x_j} = \frac{\partial}{\partial x_j}\left[\left(\nu + \frac{\nu_t}{\sigma_k}\right)\frac{\partial k}{\partial x_j}\right] + P_k - \varepsilon \tag{6}$$

$$\frac{\partial \varepsilon}{\partial t} + \frac{\partial (\varepsilon U_j)}{\partial x_j} = \frac{\partial}{\partial x_j}\left[\left(\nu + \frac{\nu_t}{\sigma_\varepsilon}\right)\frac{\partial \varepsilon}{\partial x_j}\right] + C_{\varepsilon 1}P_k\frac{\varepsilon}{k} - C_{\varepsilon 2}\frac{\varepsilon^2}{k} \tag{7}$$

$$P_k = -\overline{u_i' u_j'}\frac{\partial U_i}{\partial x_j} \tag{8}$$

where $C_{\varepsilon 1} = 1.44$, $C_{\varepsilon 2} = 1.92$, $C_\mu = 0.09$, turbulent Prandtl numbers for k and ε are $\sigma_k = 1.0$, and $\sigma_\varepsilon = 1.3$ respectively.

3.2. Boundary conditions and numerical method

In this study the ship motion and total resistance of ship were simulated by RANS based code STAR-CCM + which enables three dimensional, VOF model simulations to capture the free surface between air and water (Leroyer et al., 2011, Seo et al., 2012, Ozdemir et al., 2014). Similar computational domain was used both ship motion and ship resistance simulations. The general view of the computational domain with the model hull and the notations of boundary conditions are depicted in Fig. 2 the flow field has initially been taken as a ship length at the front of the ship, two ship lengths behind the ship and a ship length along the beam and depth directions, respectively.

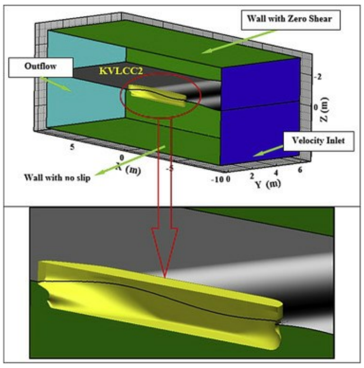

Download : Download high-res image (379KB)   Download : Download full-size image

Fig. 2. Solution domain and boundary conditions.

For the numerical solution of the governing equations, the domain is discretized in grid system (6, 254, 714), in which the mesh is clustered near the hull and free surfaces. Finite volume mesh is generated entirely with unstructured hexahedral cells as shown in Fig. 3 and the total grid points are given in Table 3. At far field, wall with slip boundary condition is used, i.e., the entire normal velocities normal to free slip wall is zero. At ship hull, wall with no slip condition and the gradient of velocity parallel to wall is zero, as the wall shear stress is zero under free slip condition. At the downstream boundary, zero second derivative for velocities in x-direction and zero gradient for free surface is used, also a hydrostatic pressure profile is specified for the outflow. At the symmetry plane boundaries zero derivative condition in the normal directions are utilized. Calculations are made in unstructured hexahedral grid computational domain for the model hull symmetric to its centerline.

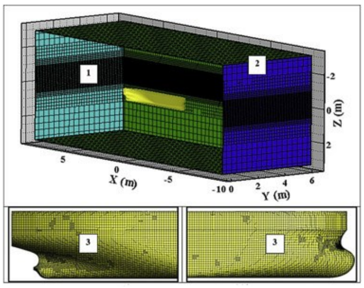

Download : Download high-res image (633KB)   Download : Download full-size image

Fig. 3. The CAD geometry and mesh of the KVLCC2 model.

Table 3. Grid analysis.

Block	Block name	Grid dimension
1	Control volume	0.1921 L_{pp}
2	Free surface	0.0960 L_{pp}
3	Near ship	0.0192 L_{pp}

There are some works used to predict the motion and the trajectory of moving underwater vehicles without the free surface effects, the detailed literature can be found at Liu and Pan (2014). At the velocity inlet boundary, the incident waves are specified as the sinusoidal wave form.

The equation for surface elevation is written as:

$$\eta = \zeta \cos\left(\mathrm{kx} - 2\pi \mathrm{f}_e \mathrm{t}\right) \tag{9}$$

The wave period T is defined as:

$$\mathrm{T} = \frac{1}{f_e} \tag{10}$$

The wavelength λ is defined as:

$$\lambda = \frac{2\pi}{\mathrm{k}} \tag{11}$$

The encounter wave frequency is given as:

$$\mathrm{f_e} = \sqrt{\frac{\mathrm{g}}{2\pi\lambda}} + \frac{\mathrm{U}}{\lambda} \tag{12}$$

where ζ is the wave amplitude, k is the wave number, U is the ship speed.

The governing equations described above are discretized using a node based finite volume method, the advection terms are discretized using a first-order upwind interpolation scheme. The governing equations are solved successively. The pressure field is solved by using the well-known SIMPLE algorithm (Patankar and Spalding, 2005). In the numerical analysis, body attached mesh method is used to simulate the ship motions.

4. Results and discussions

The main purpose of this study is to demonstrate the capability of the general-purpose CFD solver of Star CCM+ in analyzing the seakeeping characteristics by using a personal computer. The presented results for all cases are discretized for single grid and time step, based on the experience of authors' prior calculations. Due to the high computational cost, verification and validation studies are not performed. All simulations have been carried out on an eight-parallel cluster computer and it allows the approximating 6.5 million cells for simulation. Some results obtained after fifteen full days running on the computer are given in this section. To acquire the added resistance, two different computations were implemented: a calm water resistance computation and a sea-keeping computation in head waves. Both results will be presented discretely in the following sections.

4.1. Resistance test in calm water

The upstream flow velocity is taken as 1.044 m/s, which give an Fr of 0.142. The time step Δt is chosen to be 0.01 s. Fig. 4 shows how the resistance coefficients on hull converge towards unsteady solution for mesh structure. The simulations are run for a total physical flow time of 55 s, at 1.044 m/s, which corresponds to a distance of 57.4 m (approximately 10.4 ship lengths). This allows sufficient time for the free surface to develop around the hull, and permits the vessel drag force to converge to a steady value.

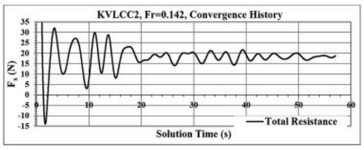

Download : Download high-res image (167KB)   Download : Download full-size image

Fig. 4. Convergence of total drag force during computation.

Concerning the calculated results, Fig. 5 shows the wave pattern around the hull, bow and stern. The Kelvin wave pattern is very clear in this picture. The resistance test results are summarized in Table 4, showing comparison of the total resistance with the experimental data. The overall agreement is very good with the experimental data and the computations of Guo et al. (2012).

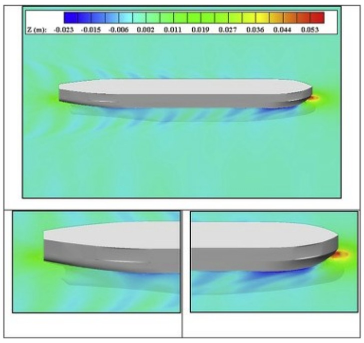

Download : Download high-res image (339KB)   Download : Download full-size image

Fig. 5. Predicted wave pattern in calm water (Fr = 0.142).

Table 4. Comparison of the total resistance.

	Experiment	Present study	Guo et al. (2012)
F_x (N)	18.20	19.00	18.67
Difference $\left\|\frac{CFD-EXP}{EXP}\right\|$ %	–	4.3%	2.60%

The y^+ variations on the ship model for Fr = 0.142 is given in Fig. 6. The precision of y^+ values on the hull determines the quality of boundary layer solution that affects the friction force. Moreover, it is seen that the y^+ values is ranged between $30 < y^+ < 160$, as essential.

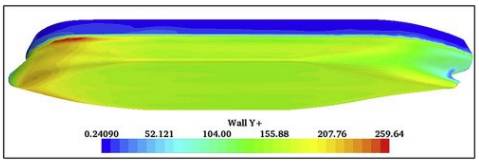

Download : Download high-res image (202KB)   Download : Download full-size image

Fig. 6. Computed y^+ distributions.

4.2. KVLCC2 pitching and heaving in head waves

The seakeeping simulations of KVLCC2 was carried out as described in Table 2. Three different conditions C1, C2 and C3 with three different wave lengths were studied. The ship is set free to pitch and heave motions. Time histories of the total resistance F_x, heave motion z and pitch angle θ are obtained from simulations. Conditions C1, C2 and C3 have frequencies of encounter of 0.761, 0.654 and 0.538, respectively. For those computations, the similar time step value of 125 time steps per wave encounter period is used. Time histories of z and θ for conditions C1, C2 and C3 are depicted in Fig. 7, Fig. 8, Fig. 9.

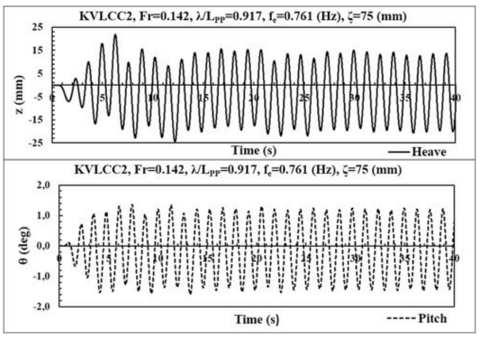

Download : Download high-res image (447KB)   Download : Download full-size image

Fig. 7. Computed time history of heave motion and pitch angle for C1.

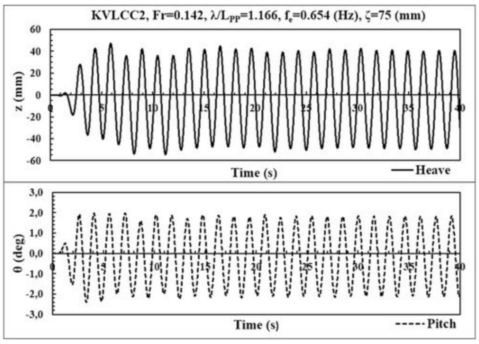

Download : Download high-res image (427KB)   Download : Download full-size image

Fig. 8. Computed time history of heave motion and pitch angle for C2.

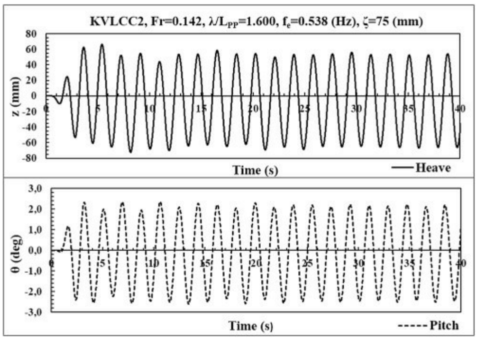

Download : Download high-res image (431KB)   Download : Download full-size image

Fig. 9. Computed time history of heave motion and pitch angle for C3.

During the first six periods, the amplitudes of the heave and pitch motions are progressively reached its maximum values. The solutions experience a permanent response. Fig. 10 shows the computed free surface elevations for the four-quarter periods.

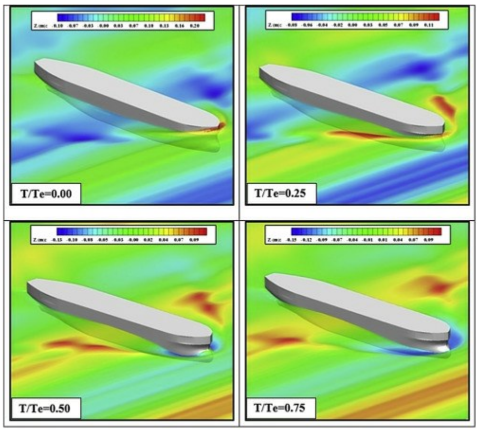

Download : Download high-res image (741KB)   Download : Download full-size image

Fig. 10. Free surface elevation for the four-quarter periods for C1.

The heave and pitch functions are approximated with Fourier Series (FS) expansions given as (Irvine et al., 2008):

$$z_I(t) = z_{I0} + z_{I1}\cos(2\pi f_e t + \gamma_{z_1}) + z_{I2}\cos(4\pi f_e t + \gamma_{z_2}) + z_{I3}\cos(6\pi f_e t + \gamma_{z_3}) \tag{13}$$

$$\theta_I(t) = \theta_{I0} + \theta_{I1}\cos(2\pi f_e t + \gamma_{\theta_1}) + \theta_{I2}\cos(4\pi f_e t + \gamma_{\theta_2}) + \theta_{I3}\cos(6\pi f_e t + \gamma_{\theta_3}) \tag{14}$$

where z_n is the heave nth order amplitude, θ_n is the pitch nth order amplitude, and γ_{z_n} and γ_{θ_n} are the phase differences.

The amplitudes of the ship's motions is obtained by the FFT analysis of the computed time history of ship's motion where the first harmonic is taken as the motion amplitude. For this unsteady analysis, the computation time is chosen as 40 s. In order to diminish the effect of sampling error on the numerical added resistance and ship motion in wave, the data in the final 10 s is used for the FFT study. Numerical and experimental FFTs of heave and pitch motions are given in Fig. 11. Numerical results in wave are compared with experimental data in Table 5.

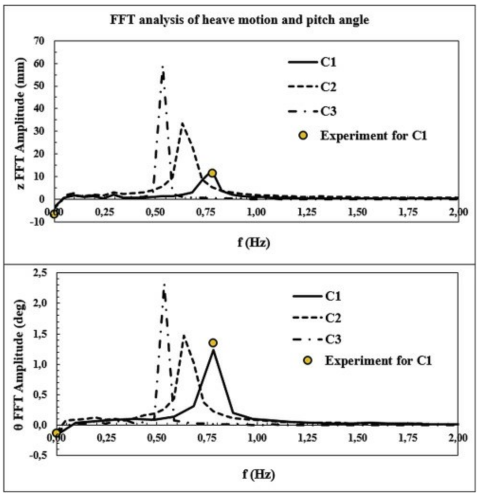

Download : Download high-res image (343KB) Download : Download full-size image

Fig. 11. FFT analysis of heave motion and pitch angle.

Table 5. Amplitudes of z and θ.

	z (mm)	θ(°)	f_e CFD
C1			0.781
0th, 1st, EFD	−6.516, 11.631	−0.137, 1.357	
0th, 1st, CFD	−3.375, 12.655	−0.120, 1.270	
0th, 1st, Difference $\left\lvert\frac{CFD-EXP}{EXP}\right\rvert$ %	48.2, 8.8	11.8, 6.3	
C2			0.634
0th, 1st, CFD	−4.030, 33.372	−0.977, 1.467	
C3			0.537
0th, 1st, CFD	−6.956, 59.333	−0.135, 2.330	

The experimental results can be obtained from G2010 (2010) and Guo et al. (2012). As can be seen from Table 5, the comparisons show that numerical calculations well predict the heave and pitch motions of KVLCC2 model. FFTs of z and θ mostly appearance robust response at the encounter frequency. The wavelength in condition C3 is very large ($\lambda/L_{PP} = 1.600$) and thus displays a very linear behavior.

4.3. Added resistance

Potential flow approach is frequently used for added resistance problems. However, for some seakeeping simulations, such as, green water calculations, slamming impact loading, breaking waves, etc., potential flow cannot handle the problem properly. In order to overcome the restrictions of strip theory, efforts to extend numerical methods for viscous flows have been made. The added resistance is calculated by the difference between mean values of the total force in waves and steady force in calm water. Steady force in calm water is given in Table 4. Fig. 12 shows the time history of the total forces on KVLCC2 model for the conditions of C1, C2 and C3.

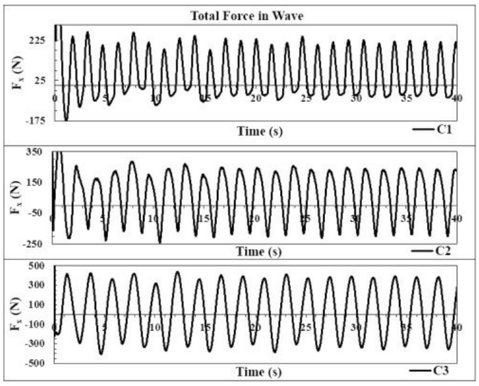

Download : Download high-res image (525KB) Download : Download full-size image

Fig. 12. Total forces on KVLCC2 model for C1, C2 and C3.

Added resistance calculation is based on following equation:

$$R_{aw} = \overline{R_{aw}} - R_{calm} \tag{15}$$

$\overline{R_{aw}}$ is the mean resistance in waves and R_{calm} is resistance in calm water. Added resistance coefficient C_{aw} is obtained and normalized according to:

$$C_{aw} = \frac{R_{aw}}{\rho g \zeta^2 B^2 / L_{pp}} \tag{16}$$

ρ is the water density, ζ is the wave amplitude of the incident waves. Fig. 13 depicts the surge forces on KVLCC2 model for C1.

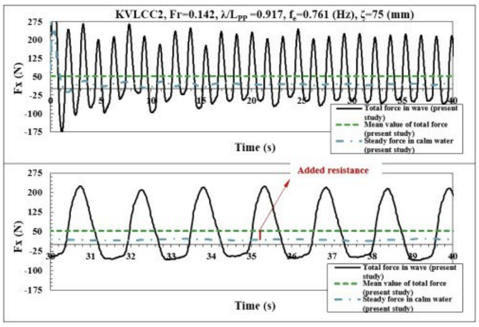

Fig. 13. Added resistance and surge force time evolution for KVLCC2 model for C1.

The y^+ variations on the ship model for the four-quarter periods for C1 is given in Fig. 14. It is seen that the y^+ values is ranged between $30 < y^+ < 300$, as required.

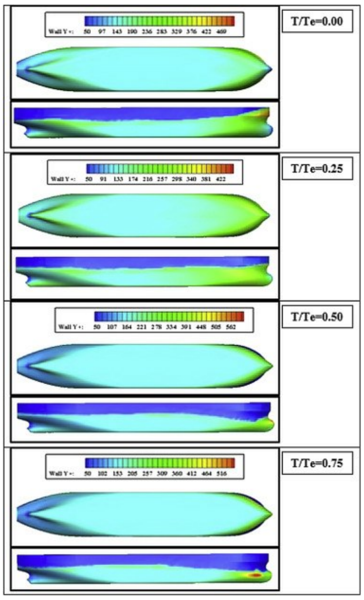

Fig. 14. y + variations for KVLCC2 model for the four-quarter periods for C1.

As previously, stated, added resistance is defined as the difference between the steady and 0th-order harmonic component of resistance. The FFT analysis of the resistance is shown in Fig. 15 0th-order harmonic which is equal the mean value of resistance can be seen from the figure. First harmonic is equal to the encounter frequency. Predicted added resistance in waves is compared with experimental data is given in Table 6.

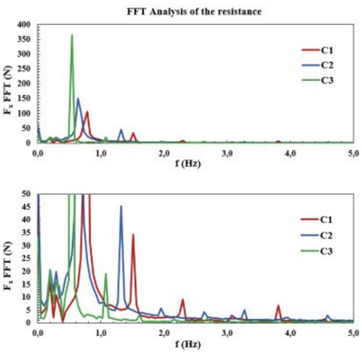

Fig. 15. FFT analysis of the resistance for C1, C2 and C3.

Table 6. Predicted added ship resistance.

	CFD			EFD		
	C1	**C2**	**C3**	**C1**	**C2**	**C3**
$\overline{R_{aw}}$ **(N)**	52.474	63.014	33.397	–	–	–
$\mathbf{R_{aw}}$ **(N)**	34.474	44.014	14.397	–	–	–
$\mathbf{C_{aw}}$	3.349	4.403	1.440	4.601	–	–

A strong non-linear behavior observed in the computed forces. The comparison with the experimental measures is not well matched for C1. The difference between predicted and experimental value is 27.2%. Nevertheless, Guo et al. (2012) reported in their study that KVLCC2 are selected as a benchmark model in the Gothenburg 2010 CFD workshop. Five groups from four countries performed the relevant calculation, and the seakeeping prediction for six wavelengths was compared. The large difference near the ship motion peak area (22.0%) reported at the Gothenburg 2010 workshop for the wavelength λ/L_{PP} = 0.9171 (C1), so it can be said that our simulation results are not large inconsistency with other CFD simulations.

5. Conclusions and future work

In this study, finite volume solution method for the RANS equations applied to the simulation of the KVLCC2 ship model for ship resistance and ship motions are studied. The main objective is to assess the performance of the commercial software Star CCM+ in analyzing the seakeeping characteristics on a personal computer. The standard $k - \varepsilon$ turbulence model is used. From the simulations of the KVLCC2 ship model, the following conclusions can be reached:

1. A value of calculated total resistance is satisfactory, with a margin of 4.3% to the experimental one.
2. Three different wave frequencies are studied. At low wave frequency, there is almost a linear response to waves.
3. The results of the first harmonic and the encounter frequency are quite well predicted for encounter frequency of 0.761.
4. The first harmonic amplitude for heave and pitch motions show good agreement with experimental results for encounter frequency of 0.761. Both heave and pitch motions, the peaks of the motion are good estimated. The poorest results occur for the 0th harmonic amplitudes where errors in 0th harmonic amplitudes for heave and pitch motions are 48.2% and 11.8% respectively for encounter frequency of 0.761. This may be due to the selection of the turbulence model. The use of a more sophisticated turbulence model can modify the results. Also strong disagreement with the experimental data may be due to the uncertainty involved in the experiment.
5. Present computations underestimate the added resistance of KVLCC2 ship model for encounter frequency of 0.761. This may indicate that the size of grid point used in the test was not sufficient for the convergence of the added resistance for the available computer power.
6. The largest added resistance is calculated around λ/L_{PP} = 1.166. Guo et al. (2012) found similar results.
7. The wavelength in condition C3 is very large (λ/L_{PP} = 1.600) and thus displays a very linear behavior.
8. A decrease in the values of y^+ by means of grids could probably have better effects on the results.
9. The given simulations are limited to regular head waves. Likewise, the simulations can be extended to other wave conditions.
10. As expected, the finer are the grids; the better is the accuracy at a cost of longer computation time. Reducing the grid size provides better representation of the bow and aft of the ship model. However, it also increases the computation time drastically, and sometimes the CPU may not be able to compute the huge amount of data because of memory deficiency. In the given simulations, the time step used depends on the encounter frequency, $\Delta t = T_e/125$. By using a more powerful computer, if the grids and time step reduces, the results would probably improve.
11. The KVLCC2 ship model has a very complex hull profile and its motion has strongly nonlinear. The results show that, the performance and ability of Star CCM + for predicting free surface flow around model ship hull generally appear good. Furthermore, different hull forms can be simulated for different wave lengths, wave amplitudes, and Froude numbers.
12. Hydrodynamic parameters (added mass, added inertia and damping ratio) can be estimated by using time series plot of ship motion study.

It was concluded that the proposed method and Star CCM + can evaluate the ship pitch and heave motions in regular head waves accurately. In addition, added resistance and response characteristics of motion in head waves can be predicted in a good margin. The estimated added resistance values can be used to calculate the EEDI (Energy Efficiency Design Index) coefficient considered on ship's design stage.

References

Arribas, 2007 F.P. Arribas
Some methods to obtain the added resistance of a ship advancing in waves
Ocean. Eng., 34 (7) (2007), pp. 946-955
View Record in Scopus Google Scholar

Chau et al., 2005 S.-W. Chau, J.-S. Kouh, T.-H. Wong, Y.-J. Chen
Investigation of hydrodynamic performance of high-speed craft rudders via turbulent flow computations, part i: non-cavitating characteristics
J. Mar. Sci. Technol., 13 (1) (2005), pp. 61-72
View Record in Scopus Google Scholar

Deng et al., 2010 G.B. Deng, M. Queutey, M. Visonneau
RANS prediction of the KVLCC2 tanker in head waves
J. Hydrodyn., 22 (5) (2010), pp. 476-481
Article Download PDF View Record in Scopus Google Scholar

Faltinsen et al., 1980 O.M. Faltinsen, K.J. Minsaas, N. Liapis, S. Skjordal
Prediction of resistance and propulsion of a ship in a seaway
Proceedings of the 13th ONR Symposium (1980)
Google Scholar

Fang, 1998 M.C. Fang
A simplified method to predict the added resistance of a SWATH ship in waves
J. Ship Res., 42 (2) (1998), pp. 131-138
CrossRef View Record in Scopus Google Scholar

Guo et al., 2012 B.J. Guo, S. Steen, G.B. Deng
Seakeeping prediction of KVLCC2 in head waves with RANS
Appl. Ocean Res., 35 (2012), pp. 56-67
Article Download PDF View Record in Scopus Google Scholar

Guo and Steen, 2011 B.J. Guo, S. Steen
Evaluation of added resistance of KVLCC2 in short waves
J. Hydrodyn., 23 (6) (2011), pp. 709-722
Article Download PDF CrossRef View Record in Scopus Google Scholar

G2010, 2010 G2010
A Workshop on CFD in Ship Hydrodynamics
(Gothenburg, Sweden)
(2010)
Google Scholar

Irvine et al., 2008 M. Irvine, J. Longo, F. Stern
Pitch and heave tests and uncertainty assessment for a surface combatant in regular head waves
J. Ship Res., 52 (2) (2008), pp. 146-163
CrossRef Google Scholar

Leroyer et al., 2011 A. Leroyer, J. Wackers, P. Queutey, E. Guilmineau
Numerical strategies to speed up CFD computations with free surface – application to the dynamic equilibrium of hulls
Ocean Eng., 38 (17–18) (2011), pp. 2070-2076
Article Download PDF View Record in Scopus Google Scholar

Liu et al., 2011 S. Liu, A. Papanikolaou, G. Zaraphonitis
Prediction of added resistance of ships in waves
Ocean Eng., 38 (4) (2011), pp. 641-650
Article Download PDF View Record in Scopus Google Scholar

Liu and Pan, 2014 T.-L. Liu, K.-C. Pan
The numerical study of the dynamic behavior of an underwater vehicle
J. Mar. Sci. Technol., 22 (2) (2014), pp. 163-172
View Record in Scopus Google Scholar

Masashi, 2013 K. Masashi
Hydrodynamic study on added resistance using unsteady wave analysis
J. Ship Res., 57 (4) (2013), pp. 220-240
Google Scholar

Matulja et al., 2011 D.J. Matulja, M. Sportelli, C. Guedes Soares, J. Prpic-Orsic
Estimation of added resistance of a ship in regular waves
Brodogradnja J. Nav. Archit. Shipbuild. Ind., 62 (3) (2011), pp. 259-264
View Record in Scopus Google Scholar

Orihara and Miyata, 2003 H. Orihara, H. Miyata
Evaluation of added resistance in regular incident waves by computational fluid dynamics motion simulation using an overlapping grid system
J. Mar. Sci. Technol., 8 (2) (2003), pp. 47-60
View Record in Scopus Google Scholar

Ozdemir et al., 2014 Y.H. Ozdemir, B. Barlas, T. Yilmaz, S. Bayraktar
Numerical and experimental study of turbulent free surface flow for a fast ship model
Brodogradnja J. Nav. Archit. Shipbuild. Ind., 65 (1) (2014), pp. 39-54
View Record in Scopus Google Scholar

Panahani et al., 2009 R. Panahani, E. Jahanbakhsh, M.S. Seif
Towards simulation of 3D nonlinear high-speed vessels motion
Ocean Eng., 36 (2009), pp. 256-265
Google Scholar

Patankar and Spalding, 2005 S.V. Patankar, D.B. Spalding
A calculation procedure for heat, mass and momentum transfer in three-dimensional parabolic flows
Int. J. Heat. Mass Transf., 15 (2) (2005), pp. 1787-1806
Google Scholar

Sadat-Hosseini et al., 2013 H. Sadat-Hosseini, P.C. Wu, P.M. Carrica
CFD verification and validation of added resistance and motions of KVLCC2 with fixed and free surge in short and long head waves
Ocean Eng., 59 (2013), pp. 240-273
Article Download PDF View Record in Scopus Google Scholar

Salvesen et al., 1970 N. Salvesen, E.O. Tuck, O.M. Faltinsen
Ship Motion and Sea Loads
SNAME (1970)
Google Scholar

Salvesen, 1978 N. Salvesen
Added resistance of ships in waves
J. Ship Hydronaut., 12 (1) (1978), pp. 24-34
CrossRef View Record in Scopus Google Scholar

Sato et al., 1999 Y. Sato, H. Miyata, T. Sato
CFD simulation of 3-dimensional motion of a ship in waves application to an advanced ship in regular heading waves
J. Mar. Sci. Technol., 4 (9) (1999), pp. 108-116
CrossRef View Record in Scopus Google Scholar

Seo et al., 2012 K.C. Seo, M. Atlar, R. Sampson
Hydrodynamic development of inclined keel hull-resistance
Ocean Eng., 47 (2012), pp. 7-18
Article Download PDF View Record in Scopus Google Scholar

Seo et al., 2013 M.G. Seo, D.M. Park, K.K. Yang
Comparative study on computation of ship added resistance in waves
Ocean Eng., 73 (2013), pp. 1-15
Article Download PDF View Record in Scopus Google Scholar

Wilson et al., 2006 R.V. Wilson, P.M. Carrica, F. Stern
Unsteady RANS method of ship motions with application to roll for a surface combatant
Comput. Fluids, 35 (2006), pp. 501-524
Article Download PDF View Record in Scopus Google Scholar

Zhirong and Decheng, 2013 S. Zhirong, W. Decheng
RANS computations of added resistance and motions of a ship in head waves
Int. J. Offshore Polar Eng., 23 (4) (2013), pp. 263-271
Google Scholar

Peer review under responsibility of Society of Naval Architects of Korea.

[1] Fax: +90 378 2278875.

View Abstract